SYNTHETIC BIOLOGY

Cell-free chemoenzymatic starch synthesis from carbon dioxide

Tao Cai[1,2]†, Hongbing Sun[1,2]†, Jing Qiao[1,2]†, Leilei Zhu[2,3]†, Fan Zhang[1,2], Jie Zhang[2,3], Zijing Tang[2,3], Xinlei Wei[2,3], Jiangang Yang[2,3], Qianqian Yuan[2,4], Wangyin Wang[5], Xue Yang[2,4], Huanyu Chu[2,4], Qian Wang[2,4], Chun You[2,3], Hongwu Ma[2,4], Yuanxia Sun[2,3], Yin Li[1,2], Can Li[5], Huifeng Jiang[2,4], Qinhong Wang[1,2,4], Yanhe Ma[1,2,3]*

Starches, a storage form of carbohydrates, are a major source of calories in the human diet and a primary feedstock for bioindustry. We report a chemical-biochemical hybrid pathway for starch synthesis from carbon dioxide (CO_2) and hydrogen in a cell-free system. The artificial starch anabolic pathway (ASAP), consisting of 11 core reactions, was drafted by computational pathway design, established through modular assembly and substitution, and optimized by protein engineering of three bottleneck-associated enzymes. In a chemoenzymatic system with spatial and temporal segregation, ASAP, driven by hydrogen, converts CO_2 to starch at a rate of 22 nanomoles of CO_2 per minute per milligram of total catalyst, an ~8.5-fold higher rate than starch synthesis in maize. This approach opens the way toward future chemo-biohybrid starch synthesis from CO_2.

S tarch is a main caloric component of food and animal feed, as well as an important industrial feedstock [1, 2]. Amylose and amylopectin polymers in starch granules consist of chains of glucosyl residues linearly linked by α-1,4-glycosidic bonds, interspersed by branching points of α-1,6-glycosidic bonds in the case of amylopectin [3]. Starch synthesis in green plants involves about 60 steps and complex regulation [4, 5]. Although many efforts have been made to improve the production of starch in plants [6–8], the inefficiency of photosynthesis and the complexity of starch biosynthesis are obstacles [9]. By contrast, advances in synthetic biology have enabled the design and construction of synthetic systems for more efficient CO_2 fixation [10–14] and chemical production [15, 16]. Inspired by the central principles of photosynthesis, extraordinary chemical catalysts have been developed to provide electrons [17] or hydrogen [18] more efficiently from solar energy and water for reducing CO_2 into simple chemicals [19, 20]. In this study, we used a chemical CO_2 reduction catalyst that produces reduced one-carbon (C1) units as an input to a chemoenzymatic pathway for cell-free starch synthesis.

To build this hybrid pathway, we first chose formic acid and methanol to serve as the candidate intermediates to bridge possible chemical catalysts and biological enzymes. We exploited formolase (fls) to design and construct the enzymatic part of the starch synthesis pathway from the candidate C1 intermediates [21]. On the basis of a main set of 6568 reactions from the MetaCyc database [22] and ATLAS database [23] and two combinatorial sets of 15 formate and 8 methanol utilization reactions, we drafted two concise starch synthesis pathways from either formic acid or methanol by using the combination of combinatorial algorithm and parsimonious flux balance analysis (comb-FBA) [24] and the COBRApy toolbox in Python [25] (fig. S1A and supplementary text). Starch could be synthesized, in principle, through only nine core reactions from CO_2 with formic acid or methanol as the C1 bridging intermediate (Fig. 1, inner circle).

In contrast to natural pathways that have evolved functionality and compatibility over hundreds of millions of years of selection, computationally designed pathways are often hindered by unpredictable and undesired interactions between enzymes from disparate biochemical contexts [26]. To overcome these problems, we pursued a strategy of modular assembly and substitution. Two starch synthesis pathways were divided into more manageable modules (fig. S1A), including a C1 module (for formaldehyde production), a C3 module (for D-glyceraldehyde 3-phosphate production), a C6 module (for D-glucose-6-phospate production), and a Cn module (for starch synthesis). According to known enzymes in databases, five modules were initially constructed (C1a/C1b, C3a, C6a, and Cna). Although the C1a, C1b, and C3a modules displayed function individually (figs. S2, A, B, and G, and S3), the

assembly of C1a or C1b with C3a did not result in detectable C3 compounds from formic acid or methanol (fig. S6A). We speculated that the marginal formaldehyde production from energy-efficient but thermodynamically unfavorable C1 modules may not be able to supply material for the key reaction of fls in the C3a module (supplementary text). We thus constructed the alternative C1 module with thermodynamically more favorable reaction cascades (fig. S2, C to E, C1c to e) [21, 27]. The most thermodynamically favorable C1e module was successfully assembled with the C3a module and achieved a substantially higher yield of C3 compounds from methanol (fig. S6A).

Assembling C1e + C3a with the C6a module (fig. S4A) produced negligible amounts of the target glucose-6-phosphate (G-6-P) (fig. S6B). We found the carbon flux was kinetically trapped at triose phosphates (fig. S8A) because of the unbalanced activity between dihydroxyacetone kinase (dak) in module C3a and fructose-6-phosphate aldolase (fsa) in module C6a (fig. S8, B and D). Furthermore, glycolaldehyde, which is the by-product of fls-catalyzed reaction in C3a, competitively inhibited the function of fsa (fig. S8, C and D, and supplementary text for more details of the incompatibilities between the C3a and C6a modules). Two alternative modules were constructed on the basis of different classes of aldolase (fig. S4, B and C, C6b and c). However, the extremely low activity of thermophilic fructose-1,6-bisphosphate aldolase/phosphatase at ambient temperature impeded the performance of C6c (table S1 and fig. S4E). For assembly of (C1e + C3a) + C6b, the function of *Escherichia coli* fructose-bisphosphatase (fbp) of module C6b was inhibited by adenosine 5′-triphosphate (ATP) and adenosine 5′-diphosphate (ADP), the essential cofactors of dak in the C3a module (fig. S9, A and B, and supplementary text). By coupling an ATP regeneration system with (C1e + C3a) + C6b [designated as (C1e + C3a) + C6b*], in which ATP was regenerated from ADP by consuming polyphosphate via polyphosphate kinase (table S1), we reduced ATP and ADP to a tolerable level and successfully produced G-6-P from methanol (figs. S9B and S6B).

Assembling C1e + C3a + C6b* with the Cna module (fig. S5A) failed to produce detectable amylose starch from methanol (fig. S6C). We observed that amylose synthesis via α-glucan phosphorylase of Cna was severely inhibited by the high inorganic phosphate (P_i)/α-D-glucose-1-phosphate (G-1-P) ratio, which could be formed from the upper part of the assembly (fig. S10, A and B, and supplementary text). Alternatively, we constructed an ATP-dependent Cnb module (fig. S5B), which is resistant to a high P_i/G-1-P ratio (fig. S10C). The assembly of (C1e + C3a + C6b*) + Cnb enabled 30 mg liter^{-1} amylose

[1]Department of Strategic and Integrative Research, Tianjin Institute of Industrial Biotechnology, Chinese Academy of Sciences, Tianjin 300308, China. [2]National Center of Technology Innovation for Synthetic Biology, Tianjin 300308, China. [3]National Engineering Laboratory for Industrial Enzymes, Tianjin Institute of Industrial Biotechnology, Chinese Academy of Sciences, Tianjin 300308, China. [4]CAS Key Laboratory of Systems Microbial Biotechnology, Tianjin Institute of Industrial Biotechnology, Chinese Academy of Sciences, Tianjin 300308, China. [5]State Key Laboratory of Catalysis, Dalian Institute of Chemical Physics, Chinese Academy of Sciences, Dalian 116023, China.
*Corresponding author. Email: ma_yh@tib.cas.cn
†These authors contributed equally to this work.

starch production from 20 mM methanol (Table 1 and fig. S6C).

With the assistance of computational pathway design and through assembling and substituting 11 modules constructed from a pool of 62 enzymes from 31 organisms (table S1), we established the artificial starch anabolic pathway (ASAP) 1.0 with 10 enzymatic reactions starting with methanol (Fig. 1, outer circle). The main intermediates and target product of ASAP 1.0 were detected by an isotopic ^{13}C-

labeling experiment (fig. S11, A and C), validating its full function for starch synthesis from methanol.

After establishing ASAP 1.0, we sought to optimize this pathway by resolving potential bottlenecks. First, because of its low kinetic activity, the enzyme fls accounted for ~86% of the total protein dosage in ASAP 1.0 to sustain the metabolic flux and maintain toxic formaldehyde at a very low level (28, 29). Directed evolution increased the fls catalytic activity,

yielding the variant fls-M3 (fls$^{I28L/T90L/N283H}$), which showed an activity improvement of 4.7-fold toward 5 mM formaldehyde and a preference of dihydroxyacetone (DHA) as the main product (fig. S12 and supplementary text).

Even though they were maintained at a low level of 1 mM with the assistance of the regeneration system, ATP and ADP may still partially inhibit the function of *E. coli* fbp (Fig. 2, B and C), which is reported to be allosterically inhibited by adenosine 5′-monophosphate

Fig. 1. Design and modular assembly of an artificial starch anabolic pathway. Inner circle: schematic of the artificial starch pathway drafted by computational pathway design with divided modules. C1 here indicates formic acid and methanol. Outer circle: schematic of artificial starch anabolic pathway (ASAP) 1.0, with individual modules colored. Auxiliary enzymes and chemicals are indicated. ADPG, ADP glucose; aox, alcohol oxidase; FADH, formaldehyde; F-1,6-BP, D-fructose-1,6-bisphosphate; F-6-P, D-fructose-6-phosphate; GAP, D-glyceraldehyde 3-phosphate; pgi, phosphoglucose isomerase; polyP, polyphosphate; pgm, phosphoglucomutase; ppa, pyrophosphatase; ppk, polyphosphate kinase; ss, starch synthase; tpi, triose-phosphate isomerase.
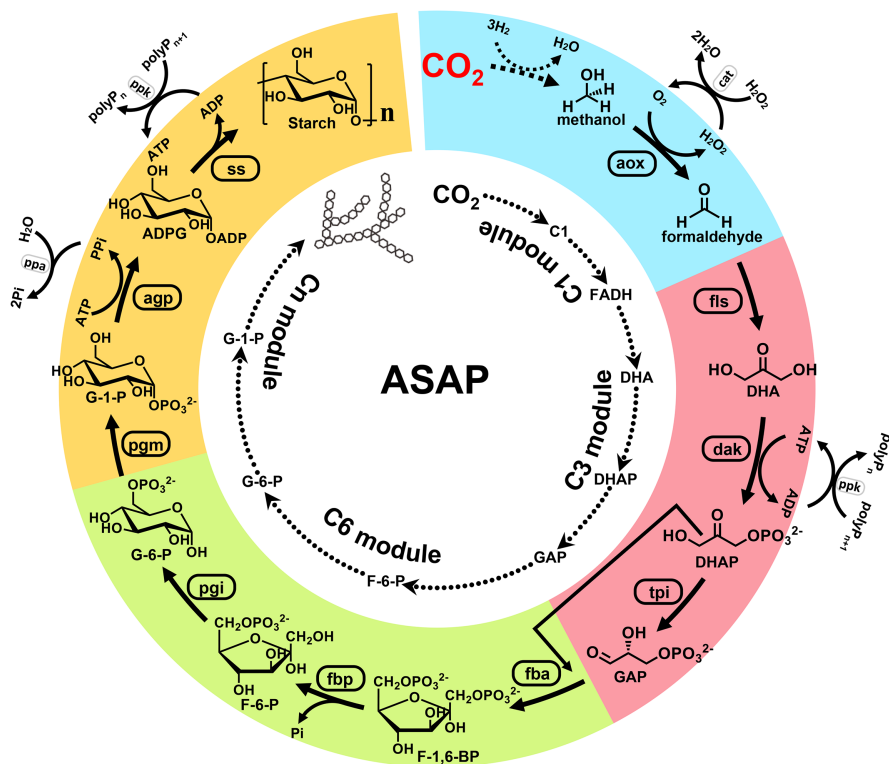
Table 1. Comparison of ASAP iterations with other natural and synthetic pathways. The average growth period of maize was assumed as 120 days. These numbers may vary depending on species, geographic location, and cultivation practices. The average molar weight of carbon unit in starch of maize was assumed as 27 g mol^{-1}. We note that starch synthesis in maize is considerably more complex than in our in vitro chemoenzymatic ASAP. For ASAP iterations, values are means, and error bars indicate SD (n = 3 replicates). NADPH, reduced form of nicotinamide adenine dinucleotide.

Pathway	Substrate	Energy input	Target product	Titer (mg liter^{-1})	Time (hours)	Productivity (mg liter^{-1} hour^{-1})	Starch synthesis rate* (nmol C min^{-1} mg^{-1})
ASAP 1.0	Methanol	–	Amylose	30 ± 1	10	3.0 ± 0.1	0.15 ± 0.01
ASAP 2.0	Methanol	–	Amylose	230 ± 5	10	23 ± 1	2.0 ± 0.1
ASAP 3.0	CO$_2$	H$_2$	Amylose	1640 ± 86	4	410 ± 22	22 ± 1†
ASAP 3.1	CO$_2$	H$_2$	Amylopectin	1280 ± 6	4	320 ± 2	17.2 ± 0.1†
CETCH 5.4	NaHCO$_3$	NADPH	Glyoxylate	40.0	1.5	26.7	3.87‡
Calvin cycle (maize)	CO$_2$ and H$_2$O	Solar	Starch	–	120 days	–	2.58§

*Starch synthesis rate was calculated for the indicated substrates and shown as a nanomole of carbon converted to product per minute per milligram of total proteins. †The rate was calculated by using total amount of both catalyst and proteins (see supplementary materials). ‡The end product of CETCH is glyoxylate. Rate of CETCH was recalculated with 3.1 mg ml^{-1} of total proteins (13). §Calculation mainly based on reported data that starch is 26.1% of total biomass and total proteins, excluding storage protein in grain, are 2.17% of total biomass (40).

(AMP) (30). We found that the variant fbp-A^R (fbp$^{K104Q/R132I}$), which contains two mutations in the AMP allosteric site (31), alleviated ADP inhibition (Fig. 2, B and C) and substantially improved G-6-P production from DHA (Fig. 2D). Analysis of the inhibition pattern of the three kinds of nucleotide on fbp and fbp-A^R indicated that ATP or ADP was the determinant for inhibition in the system (table S5 and supplementary text). By integrating fbp-A^R with a reported variant resistant to G-6-P (31), a combined variant fbp-AG^R (fbp$^{K104Q/R132I/Y210F/K218Q}$) enabled a further improvement (Fig. 2D and supplementary text).

ATP competition between dak and ADP-glucose pyrophosphorylase (agp) was considered, as an increase in substrate DHA and its kinase dak resulted in an aberrantly lower starch production during the first 4 hours (Fig. 2A and fig. S10D). We confirmed that the co-existence of DHA and dak severely inhibited

starch synthesis via Cnb (Fig. 2E) and output DHA phosphate (DHAP) as the dominant product over starch (Fig. 2F, first column), which validates that dak competitively consumed most of the ATP. Instead of reducing the dosage of dak, we tried to enhance the capacity of agp. Three high-activity agp variants were created in accordance with reported amino acid substitutions (32, 33), and these variants displayed enhanced competition against dak (Fig. 2F). The best variant, agp-M3, successfully increased starch synthesis from DHA by approximately sixfold (Fig. 2G).

Using these three engineered enzymes (fls-M3, fbp-AG^R, and agp-M3), we constructed ASAP 2.0, which produced ~230 mg liter^{-1} amylose starch in 10 hours from 20 mM methanol (Table 1). Compared with that of ASAP 1.0, the starch productivity of ASAP 2.0 was improved 7.6-fold. On the basis of ^{13}C-labeling liquid chromatography–mass spectrometry (LC-MS)

analysis, ASAP 2.0 accumulated a lower concentration of intermediates than ASAP 1.0 (fig. S11, A and B), which indicates the effectiveness of our optimization strategies.

With the above success in ASAP 2.0, we proceeded to synthesize starch from CO_2 and hydrogen by coupling the enzymatic processes with CO_2 reduction by means of a previously developed inorganic catalyst, ZnO-ZrO$_2$ (34). Because of the unfavorable conditions of CO_2 hydrogenation, we developed a chemoenzymatic cascade system in ASAP 3.0 with a chemical reaction unit and an enzymatic reaction unit. To satisfy the demand of fls for a high concentration of formaldehyde and to avoid its toxicity to other enzymes (fig. S13), we further operated the enzymatic unit with two steps (Fig. 3A). In the chemical reaction unit, CO_2 was chemically hydrogenated to methanol at a rate of ~0.25 g hour^{-1} g^{-1} catalyst, and the produced methanol was constantly condensed
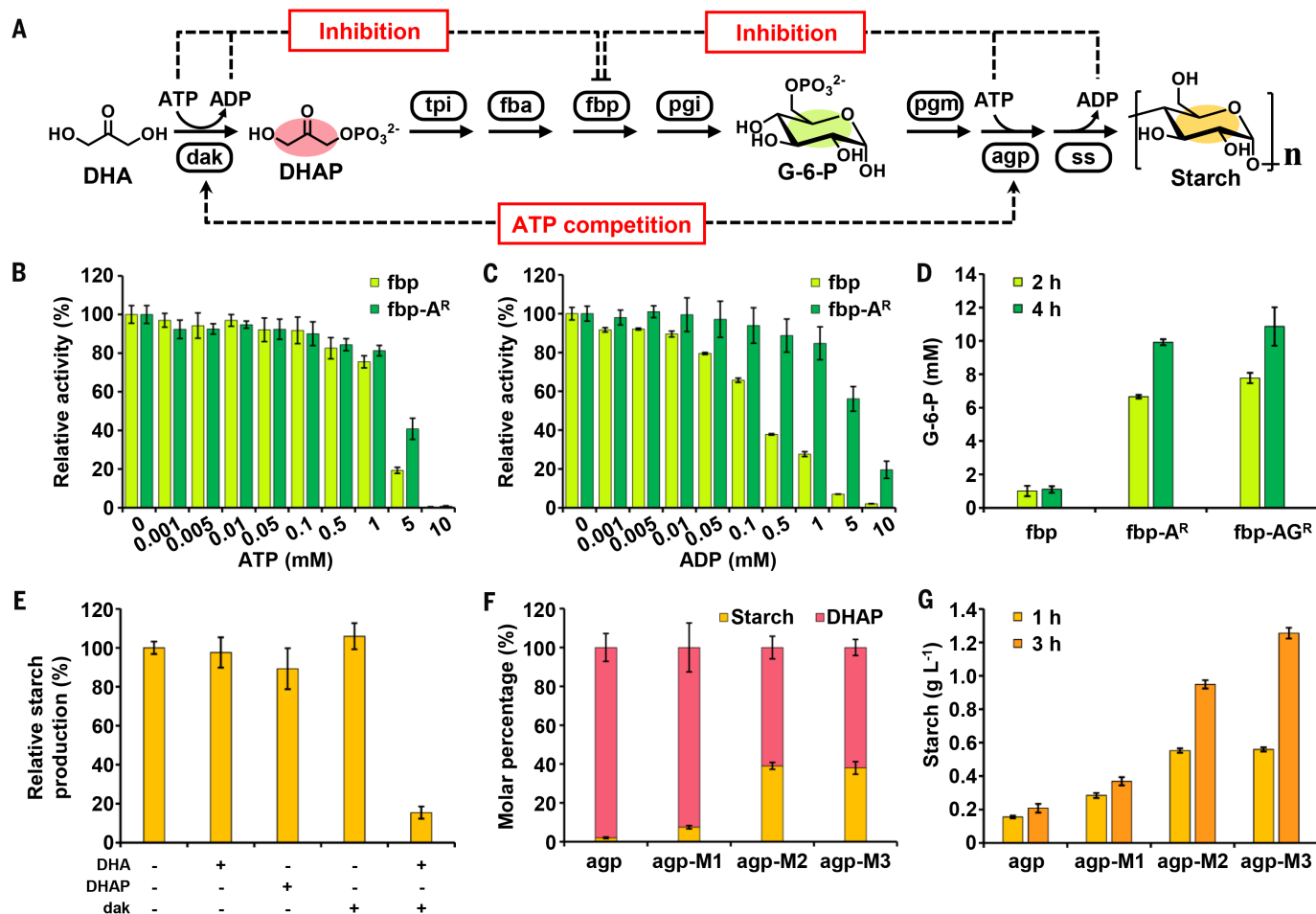
Fig. 2. Resolving main bottlenecks in ASAP. (**A**) Partial ASAP pathway from DHA to starch with bottlenecks indicated and key intermediates and product colored. (**B** and **C**) Inhibitory effect of ATP and ADP on fbp and fbp-A^R. (**D**) G-6-P production from 25 mM DHA via pathway with different fbp variants. (**E**) Inhibition by components from C3a model on the Cnb model. DHA, DHAP, and dak were present at concentrations of 25 mM, 10 mM, and 0.2 mg ml^{-1}, respectively. (**F**) Proportion of DHAP and starch (in glucose) produced from 25 mM DHA and 10 mM G-6-P in a competitive system, which includes dak and the Cnb module, with different agp variants. (**G**) Starch (in glucose) production from 25 mM DHA via partial ASAP as depicted in Fig. 2A. For (B) to (G), values are means, and error bars indicate SD (n = 3 replicates).

and fed into the enzymatic unit to a final concentration of ~100 mM during the first hour. In the enzymatic unit, the methanol was first converted to ~22.5 mM C3 intermediate DHA for another 1 hour by supplementing two core enzymes and auxiliary catalase (cat) and then transformed to ~1.6 g liter^{-1} amylose starch in the subsequent 2 hours by supplementing the remaining eight core enzymes and auxiliary components (Fig. 3A). The synthetic amylose exhibited the same deep blue color and absorption maximum as standard amylose in the presence of iodine solution (Fig. 3B).

Natural starch contains ~20 to 30% amylose and 70 to 80% amylopectin (3). To synthesize amylopectin from CO_2, we introduced a starch branching enzyme (sbe) from *Vibrio vulnificus* (35) in ASAP 3.1. This setup produced ~1.3 g liter^{-1} amylopectin within 4 hours (Fig. 3A). The synthetic amylopectin had a reddish-brown color and a comparable absorption maximum as standard amylopectin after iodine treatment (Fig. 3B). Both the synthetic amylose and amylopectin exhibited the same one to six proton nuclear magnetic resonance signals as their standard counterparts (Fig. 3, C and D).

By using spatial and temporal segregation of steps, ASAP 3.0 achieved a high starch productivity of ~410 mg liter^{-1} hour^{-1} from CO_2. The starch synthesis rate of this chemoenzymatic pathway reached 22 nmol min^{-1} mg^{-1} of total catalyst and proteins, which is an 8.5-fold higher rate than that of starch synthesis via the Calvin cycle in maize (Table 1). This rate is also 5.7-fold higher than that of the synthetic crotonyl–coenzyme A (CoA)/ethylmalonyl-CoA/hydroxybutyryl-CoA (CETCH) cycle which has been recently extended into a platform to access different compounds directly from CO_2 (12, 13, 36). The theoretical hydrogen-to-methanol energy efficiency (η_{HME}) and methanol-to-starch energy efficiency (η_{MSE}) of ASAP is 85 and 61%, respectively, although these values do not consider energy consumption for processes such as enzyme production and maintenance of high temperature and pressure in the chemical step (supplementary text), which will compromise the energy efficiency of ASAP in practice. With an attainable solar-to-electricity efficiency (η_{SEE}) of 20% (17) and electricity-to-hydrogen efficiency (η_{EHE}) of 85% (18) in ideal photovoltaic and water-electrolysis devices, the theoretical maximal solar-to-starch efficiency ($\eta_{SSE} = \eta_{SEE} \times \eta_{EHE} \times \eta_{HME} \times \eta_{MSE}$) via ASAP will be 9%. With the estimated practical η_{HME}' of 68% considering the energy for temperature and pressure in the chemical step (37), the theoretical η_{SSE} is adjusted to 7%, which is comparable to the theoretical photosynthetic efficiency of solar energy to biomass for C3 (4.6%) and
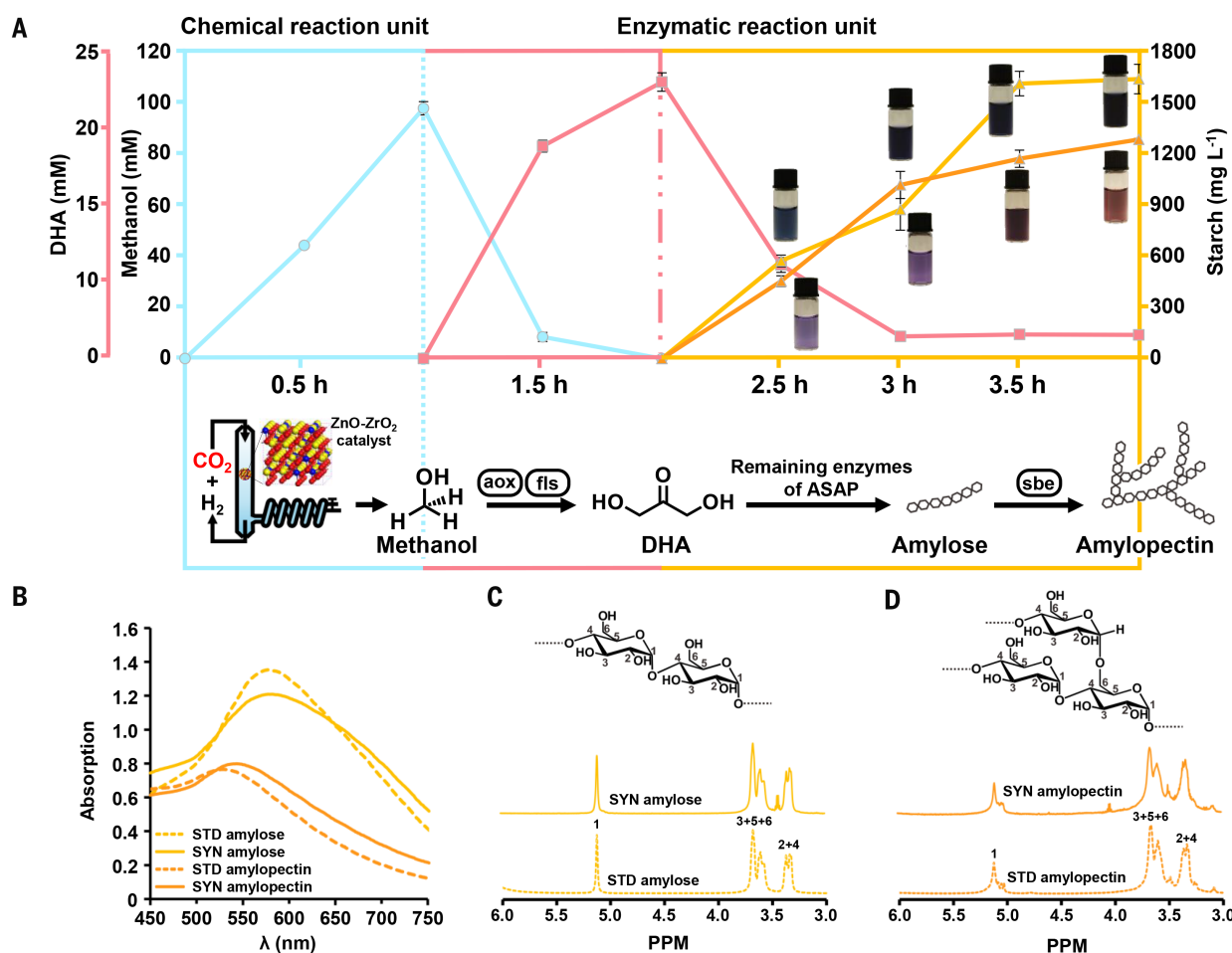
Fig. 3. Starch synthesis via ASAP from CO_2. (A) (Bottom) Time course of chemoenzymatic cascade reactions for starch synthesis from CO_2. sbe, starch branching enzyme. (Top) Alteration of key intermediates and starch (yellow curve indicating amylose and orange curve indicating amylopectin) during the time course. The production of amylose and amylopectin are also visualized in the vials by iodine dyeing at given time points. The reaction solution was diluted sixfold before iodine treatment. Values are means, and error bars indicate SD (n = 3 replicates). **(B)** Absorption spectra analysis of synthetic amylose and amylopectin after iodine treatment. The wavelength of maximum absorption (λ_{max}) of standard (STD) and synthetic (SYN) amylose is 577 nm and λ_{max} of standard and synthetic amylopectin is 529 and 543 nm, respectively. **(C** and **D)** ^{1}H nuclear magnetic resonance (NMR) spectrum of standard (STD) and synthetic (SYN) amylose and amylopectin.

C4 (6%) plants (*38*) and is 3.5 fold of the estimated theoretical solar-to-starch efficiency for plants (2%) in a natural environment (*39*). Cell-free, chemoenzymatic, and efficient starch synthesis from CO_2 by ASAP provides an important starting point for applications such as industrial biomanufacturing of starch.

REFERENCES AND NOTES

1. P. L. Keeling, A. M. Myers, *Annu. Rev. Food Sci. Technol.* **1**, 271–303 (2010).
2. R. Höfer, "Sugar- and starch-based biorefineries" in *Industrial Biorefineries and White Biotechnology*, A. Pandey, R. Höfer, M. Taherzadeh, M. Nampoothiri, C. Larroche, P. L. Keeling, A. M. Myers, Eds. (Elsevier, 2015), chap. 4A, pp. 157–235.
3. R. L. Whistler, J. R. Daniel, "Molecular structure of starch" in *Starch: Chemistry and Technology*, R. L. Whistler, J. N. Bemiller, E. F. Paschall, Eds. (Academic Press, ed. 2, 1984), pp. 153–182.
4. T. Saithong, A. Meechai, S. Cheevadhanarak, S. Bhumiratana, *J. Comput. Sci. Syst. Biol.* **5**, 24–37 (2012).
5. M. R. Abt, S. C. Zeeman, *Curr. Opin. Plant Biol.* **55**, 109–117 (2020).
6. J. Li *et al.*, *Plant Cell Physiol.* **54**, 282–294 (2013).
7. N. Li, S. Zhang, Y. Zhao, B. Li, J. Zhang, *Planta* **233**, 241–250 (2011).
8. M. Hakata *et al.*, *Plant Biotechnol. J.* **10**, 1110–1117 (2012).
9. A. Bahaji *et al.*, *Biotechnol. Adv.* **32**, 87–106 (2014).
10. A. Bar-Even, E. Noor, N. E. Lewis, R. Milo, *Proc. Natl. Acad. Sci. U.S.A.* **107**, 8889–8894 (2010).
11. A. Satanowski *et al.*, *Nat. Commun.* **11**, 5812 (2020).
12. M. Scheffen *et al.*, *Nat. Catal.* **4**, 105–115 (2021).
13. T. Schwander, L. Schada von Borzyskowski, S. Burgener, N. S. Cortina, T. J. Erb, *Science* **354**, 900–904 (2016).
14. T. E. Miller, *Science* **368**, 649–654 (2020).
15. T. P. Korman, P. H. Opgenorth, J. U. Bowie, *Nat. Commun.* **8**, 15526 (2017).
16. S. Sherkhanov *et al.*, *Nat. Commun.* **11**, 4292 (2020).
17. M. Green *et al.*, *Prog. Photovolt. Res. Appl.* **29**, 3–15 (2021).
18. S. Shiva Kumar, V. Himabindu, *Mater. Sci. Energy Technol.* **2**, 442–454 (2019).
19. Y. Y. Birdja *et al.*, *Nat. Energy* **4**, 732–745 (2019).
20. R.-P. Ye *et al.*, *Nat. Commun.* **10**, 5698 (2019).
21. J. B. Siegel *et al.*, *Proc. Natl. Acad. Sci. U.S.A.* **112**, 3704–3709 (2015).
22. R. Caspi *et al.*, *Nucleic Acids Res.* **44**, D471–D480 (2016).
23. N. Hadadi, J. Hafner, A. Shajkofci, A. Zisaki, V. Hatzimanikatis, *ACS Synth. Biol.* **5**, 1155–1166 (2016).
24. X. Yang *et al.*, *Metab. Eng.* **56**, 142–153 (2019).
25. A. Ebrahim, J. A. Lerman, B. O. Palsson, D. R. Hyduke, *BMC Syst. Biol.* **7**, 74 (2013).
26. T. J. Erb, P. R. Jones, A. Bar-Even, *Curr. Opin. Chem. Biol.* **37**, 56–62 (2017).
27. A. Chou, J. M. Clomburg, S. Qian, R. Gonzalez, *Nat. Chem. Biol.* **15**, 900–906 (2019).
28. Y. S. Tai, K. Zhang, *Nat. Chem. Biol.* **11**, 384–386 (2015).
29. S. Poust *et al.*, *ChemBioChem* **16**, 1950–1954 (2015).
30. J. K. Hines, C. E. Kruesel, H. J. Fromm, R. B. Honzatko, *J. Biol. Chem.* **282**, 24697–24706 (2007).
31. J. S. Yang, S. W. Seo, S. Jang, G. Y. Jung, S. Kim, *PLOS Comput. Biol.* **8**, e1002612 (2012).
32. C. R. Meyer, J. A. Bork, S. Nadler, J. Yirsa, J. Preiss, *Arch. Biochem. Biophys.* **353**, 152–159 (1998).
33. C. R. Meyer, J. Yirsa, B. Gott, J. Preiss, *Arch. Biochem. Biophys.* **352**, 247–254 (1998).
34. J. Wang *et al.*, *Sci. Adv.* **3**, e1701290 (2017).
35. H. J. Jo, S. Park, H. G. Jeong, J. W. Kim, J. T. Park, *FEBS Lett.* **589**, 1089–1094 (2015).
36. S. Sundaram *et al.*, *Angew. Chem. Int. Ed.* **60**, 16420–16425 (2021).
37. E. S. Van-Dal, C. Bouallou, *J. Clean. Prod.* **57**, 38–45 (2013).
38. X. G. Zhu, S. P. Long, D. R. Ort, *Curr. Opin. Biotechnol.* **19**, 153–159 (2008).
39. Y. H. P. Zhang, C. You, H. Chen, R. Feng, "Surpassing photosynthesis: high-efficiency and scalable CO_2 utilization through artificial photosynthesis" in *Recent Advances in Post-Combustion CO_2 Capture Chemistry*. M. Attalla, Ed. (American Chemical Society, 2012), pp. 275–292.
40. C. S. Kuehn, J. G. Linn, D. G. Johnson, H. G. Jung, M. I. Endres, *J. Dairy Sci.* **82**, 2746–2755 (1999).

Science

Cell-free chemoenzymatic starch synthesis from carbon dioxide

Tao CaiHongbing SunJing QiaoLeilei ZhuFan ZhangJie ZhangZijing TangXinlei WeiJiangang YangQianqian YuanWangyin WangXue YangHuanyu ChuQian WangChun YouHongwu MaYuanxia SunYin LiCan LiHuifeng JiangQinhong WangYanhe Ma

From carbon dioxide to starch: no plants required

Many plants turn glucose from photosynthesis into polymers that form insoluble starch granules ideal for long-term energy storage in roots and seeds. Cai *et al.* developed a hybrid system in which carbon dioxide is reduced to methanol by an inorganic catalyst and then converted by enzymes first to three and six carbon sugar units and then to polymeric starch. This artificial starch anabolic pathway relies on engineered recombinant enzymes from many different source organisms and can be tuned to produce amylose or amylopectin at excellent rates and efficiencies relative to other synthetic carbon fixation systems—and, depending on the metric used, even to field crops. —MAF

View the article online
https://www.science.org/doi/10.1126/science.abh4049
Permissions
https://www.science.org/help/reprints-and-permissions

Use of think article is subject to the Terms of service